nature immunology

# The ubiquitin-modifying enzyme A20 restricts ubiquitination of the kinase RIPK3 and protects cells from necroptosis

Michio Onizawa[1,6], Shigeru Oshima[1,5,6], Ulf Schulze-Topphoff[2,6], Juan A Oses-Prieto[3], Timothy Lu[1], Rita Tavares[1], Thomas Prodhomme[2], Bao Duong[1], Michael I Whang[1], Rommel Advincula[1], Alex Agelidis[1], Julio Barrera[1], Hao Wu[4], Alma Burlingame[3], Barbara A Malynn[1], Scott S Zamvil[2] & Averil Ma[1]

**A20 is an anti-inflammatory protein linked to multiple human diseases; however, the mechanisms by which A20 prevents inflammatory disease are incompletely defined. We found that A20-deficient T cells and fibroblasts were susceptible to caspase-independent and kinase RIPK3–dependent necroptosis. Global deficiency in RIPK3 significantly restored the survival of A20-deficient mice. A20-deficient cells exhibited exaggerated formation of RIPK1-RIPK3 complexes. RIPK3 underwent physiological ubiquitination at Lys5 (K5), and this ubiquitination event supported the formation of RIPK1-RIPK3 complexes. Both the ubiquitination of RIPK3 and formation of the RIPK1-RIPK3 complex required the catalytic cysteine of A20's deubiquitinating motif. Our studies link A20 and the ubiquitination of RIPK3 to necroptotic cell death and suggest additional mechanisms by which A20 might prevent inflammatory disease.**



A20 is a deubiquitinating enzyme that inhibits activation of the transcription factor NF-κB and restricts apoptosis induced by tumor-necrosis factor (TNF)[1–4]. A20 is a potent anti-inflammatory protein linked to multiple human autoimmune diseases and to human malignancies[5,6]. Polymorphisms in the human *TNFAIP3* gene (which encodes A20 protein) are associated with reduced function or expression of A20 that confers susceptibility to autoimmune diseases[7,8]. Deletion of A20 in mice leads to widespread tissue inflammation and perinatal death[2]. A20 regulates multiple signaling cascades and has distinct physiological functions in different cell types[5,6]. In myeloid cells, A20 prevents inflammation by restricting signaling downstream of NF-kB, from Toll-like receptors, the receptor Nod2 and other receptors of the innate immune system[4,9–14]. These signals lead to the production of pro-inflammatory cytokines such as interleukin 6 (IL-6) and TNF as well as co-stimulatory molecules that activate lymphocytes and cells of the innate immune system that lead to autoimmune and inflammatory diseases. In A20-deficient B cells, exaggerated activation of NF-κB triggered by the B cell antigen receptor and the costimulatory receptor CD40 leads to increased B cell survival and autoimmunity[15–17]. Hence, A20 inhibits activation of NF-κB in various cell types to prevent inflammatory and autoimmune diseases.

The biochemical mechanisms by which A20 restricts signals that lead to the activation of NF-κB are complex and incompletely understood. Ubiquitination of signaling proteins can facilitate their recruitment to non-degradative signaling complexes, often mediated by Lys63 (K63)-linked or linear polyubiquitin chains[18]. A20 is an unusual protein that utilizes two distinct motifs to remove activating K63-linked polyubiquitin chains from substrates and build degradative K48-linked ubiquitin chains[3,4,19,20]. A20 may also disrupt interactions between the ubiquitin-conjugating enzyme E2 and ubiquitin ligases E3 by destabilizing E2 enzymes[21]. A20 also has ubiquitin-binding motifs that support its interaction with the kinase RIPK1, E2 and the kinase IKKγ[19,22–25]. In addition, A20 binds members of the E3 family of ubiquitin ligases (such as TRAF2 and TRAF6), ubiquitin sensors (such as ABIN-1 and ABIN-2), and other proteins (such as TAX1BP1) that may act together with A20 to achieve its critical biochemical functions[26]. A20's motifs and protein interactions suggest that A20 regulates multiple signaling cascades by modifying the ubiquitination of key signaling proteins.

Here we investigated the physiological function of A20 in mouse T cells. We observed decreased population expansion of A20-deficient T cells due to exaggerated cell death and identified a previously unknown function for A20 in protecting T cells against necroptosis, a caspase-independent form of programmed cell death. T cell–specific deficiency in RIPK3 restored the survival of A20-deficient T cells, and global deficiency in RIPK3 partially rescued A20-deficient mice (*Tnfaip3*$^{-/-}$ mice; called '*A20*$^{-/-}$' mice here) from the perinatal death caused by A20 deficiency. Ubiquitination of RIPK3 at Lys5 (K5)

[1]Department of Medicine, University of California, San Francisco, San Francisco, California, USA. [2]Department of Neurology, University of California, San Francisco, San Francisco, California, USA. [3]Department of Pharmaceutical Chemistry, University of California, San Francisco, San Francisco, California, USA. [4]Program in Cellular and Molecular Medicine, Boston Children's Hospital, Department of Biological Chemistry and Molecular Pharmacology, Harvard Medical School, Boston, Massachusetts, USA. [5]Present address: Department of Gastroenterology and Hepatology, Tokyo Medical and Dental University, Tokyo, Japan. [6]These authors contributed equally to this work. Correspondence should be addressed to A.M. (averil.ma@ucsf.edu).

Received 23 January; accepted 8 April; published online 4 May 2015; corrected after print 21 May 2015; doi:10.1038/ni.3172

supported formation of the RIPK1-RIPK3 complex and necroptosis. A20 used its deubiquitinating motif to restrict the ubiquitination of RIPK3 and the formation of necroptotic RIPK1-RIPK3 complexes.

## RESULTS

### A20 supports the survival of activated T cells

Mice with *lox*P-flanked exon 2 of alleles encoding A20 ($A20^{fl/fl}$) deleted by Cre recombinase expressed from the T cell–specific *Cd4* promoter ($A20^{fl/fl}$CD4-Cre mice) developed normally and survived for at least 6 months without gross disease (data not shown), which suggested that conditional, T cell–specific deletion of A20 did not profoundly perturb cellular immunological homeostasis. The number and frequency of $CD4^+CD8^+$ double-positive thymocytes and $CD8^+$ or $CD4^+$ single-positive thymocytes were normal (data not shown). The total number of splenic T cells in $A20^{fl/fl}$CD4-Cre mice was similar to that in control $A20^{+/fl}$CD4-Cre mice and $A20^{+/+}$CD4-Cre mice (**Fig. 1a** and data not shown), which suggested that T cell development occurred normally in the absence of A20. Analysis of T cell–activation markers revealed a greater frequency of T cells with a memory phenotype ($CD44^{hi}CD62^{lo}$) in $A20^{fl/fl}$CD4-Cre mice than in $A20^{+/fl}$CD4-Cre mice (**Fig. 1b**), which suggested a role for A20 in regulating T cell responses following exposure to antigen. Spontaneous activation of T cells in $A20^{fl/fl}$CD4-Cre mice was accompanied by modestly increased number of myeloid cells ($Mac\text{-}1^+Gr1^+$), but not B cells ($CD19^+$), compared with that in $A20^{+/fl}$CD4-Cre mice (**Fig. 1a**). We observed no difference between $A20^{+/fl}$CD4-Cre mice and $A20^{+/+}$ CD4-Cre mice in any of these parameters (data not shown), so we used $A20^{+/fl}$CD4-Cre mice as controls in subsequent experiments.

To investigate the role of A20 in T cell responses, we purified naive $CD4^+$ T cells from $A20^{fl/fl}$CD4-Cre and $A20^{+/fl}$CD4-Cre mice and stimulated these cells via the T cell antigen receptor (TCR) with antibody to the invariant signaling protein CD3 (anti-CD3) and antibody to the coreceptor CD28 (anti-CD28). $A20^{fl/fl}$CD4-Cre T cells were activated as readily as $A20^{+/fl}$CD4-Cre cells were, as indicated by expression of the activation markers CD69 and CD44 and by expression of IL-2 (data not shown). $A20^{fl/fl}$CD4-Cre T cells stimulated via the TCR diluted the division-tracking dye CFSE more than their $A20^{+/fl}$ CD4-Cre counterparts did (**Fig. 1c**), which indicated that activated A20-deficient $CD4^+$ T cells cycled more than $A20^{+/fl}$CD4-Cre T cells did. However, the frequency of $A20^{fl/fl}$CD4-Cre T cells among total live T cells on days 2 and 3 after stimulation was markedly lower than that of $A20^{+/fl}$CD4-Cre cells (**Fig. 1d**), which indicated that A20 deficiency impaired the survival of activated T cells in a cell-autonomous fashion. To normalize potential differences in cytokine production and investigate the cell-autonomous role of A20 in regulating T cell function, we interbred $A20^{fl}$CD4-Cre mice with $CD45.1^+$ congenic mice and stimulated equal (1:1) mixtures of sorted naive congenic $A20^{fl/fl}$CD4-Cre $CD4^+$ T cells and $A20^{+/fl}$CD4-Cre $CD4^+$ T cells *in vitro*. In these mixed cultures, both A20-deficient and A20-sufficient T cells were exposed to the same amounts of IL-2 and other T cell–derived cytokines. These experiments confirmed that $A20^{fl/fl}$CD4-Cre T cell populations expanded poorly relative to $A20^{+/fl}$ CD4-Cre $CD4^+$ T cell populations (data not shown). To eliminate the possibility of potential development defects contributed by A20 deficiency and to confirm that A20 directly regulated the survival of mature peripheral T cells, we interbred $A20^{fl/fl}$ mice with ROSA26-ER-Cre mice to allow 4-OH-tamixifen–inducible deletion of the gene encoding A20. The resultant $A20^{fl/fl}$ROSA26-ER-Cre mice had normal lymphoid populations (data not shown). We sorted naive $CD4^+$ T cells from $A20^{fl/fl}$ROSA26-ER-Cre mice and control $A20^{+/fl}$ROSA26-ER-Cre mice, mixed the cells and stimulated them for 3 d *in vitro* with anti-CD3 and anti-CD28 in the presence of 4-OH-tamixifen to induce efficient deletion of A20 (**Supplementary Fig. 1**). Such 'acute' deletion of A20 resulted in greater death of $A20^{fl/fl}$ROSA26-ER-Cre T cells than of $A20^{+/fl}$ROSA26-ER-Cre T cells (**Fig. 1e**), which suggested that A20 directly supported the survival of activated T cells.

### Increased RIPK1-RIPK3 complexes in A20-deficient T cells

Activated A20-deficient B cells express increased amounts of the anti-apoptotic factor Bcl-x, which renders them resistant to death mediated by the death receptor Fas (CD95)[15]. To investigate how A20 protects the survival of activated T cells, we assessed the expression of proteins of the antiapoptotic Bcl-2 family in A20-deficient T cells. Immunoblot analysis revealed that the expression of Bim, Bax, Bcl-x and Bcl-2 was similar in activated $A20^{fl/fl}$CD4-Cre T cells and $A20^{+/fl}$CD4-Cre T cells (**Fig. 2a**). We also observed that more $A20^{fl/fl}$CD4-Cre T cells than $A20^{+/fl}$CD4-Cre T cells died after blockade of TNF, Fas or interferon-γ (IFN-γ) (**Fig. 2b**), which suggested that the death of A20-deficient cells was not triggered by these stimuli. Notably, the pan-caspase inhibitors Z-VAD or Q-VD did not abrogate the increased susceptibility of stimulated $A20^{fl/fl}$CD4-Cre $CD4^+$ T cells to death, compared with that of $A20^{fl/+}$CD4-Cre $CD4^+$ T cells (**Fig. 2b**); this indicated the involvement of a caspase-independent death pathway.

Activated T cells die by necroptosis in the absence of the pro-apoptotic proteins FADD or caspase-8 (refs. 27,28). Necroptosis requires the kinase activity of RIPK1 and the formation of RIPK1-RIPK3 complexes[29–31]. The RIPK1-kinase-activity inhibitor necrostatin-1 selectively restored the survival and population expansion of $A20^{fl/fl}$CD4-Cre T cells activated via the TCR, compared with that of activated $A20^{+/fl}$CD4-Cre T cells (**Fig. 2b**), while an inactive form of necrostatin-1 was less effective in restoring the survival of $A20^{fl/fl}$CD4-Cre T cells (**Supplementary Fig. 2**). Thus, the kinase activity of RIPK1 contributed to the increased death of A20-deficient T cells following *in vitro* activation.

Immunoprecipitation of RIPK1 from $CD4^+$ T cells activated via the TCR revealed that $A20^{fl/fl}$CD4-Cre T cells contained significantly greater amounts of RIPK1-associated RIPK3 than $A20^{+/fl}$CD4-Cre T cells did (**Fig. 2c**), which indicated that RIPK1-RIPK3 complexes accumulated in A20-deficient T cells and suggested that A20 protected activated T cells from necroptotic death. To further identify the role of RIPK3 in mediating the increased death of $A20^{fl/fl}$CD4-Cre T cells, we interbred $A20^{fl/fl}$CD4-Cre mice with $Ripk3^{-/-}$ mice. Following *in vitro* stimulation of the TCR for 72 or 120 h in the presence of Z-VAD, the number of $A20^{fl/fl}$CD4-Cre $Ripk3^{-/-}$ T cells was greater than that of $A20^{fl/fl}$ T cells, although it was less than that of control $A20^{+/fl}$ T cells (**Fig. 2d**), which indicated that RIPK3 deficiency significantly restored the survival of activated A20-deficient T cells. The viability of caspase-8-deficient Jurkat I9.2 human T cells stimulated via the TCR was reduced for cells treated with A20-specific small interfering RNA (siRNA) relative to that of their counterparts treated with control siRNA, and RIPK3-specific siRNA abrogated the increased death of A20-deficient Jurkat I9.2 T cells observed (**Fig. 2e**), which suggested that the epistatic relationship between A20 and RIPK3 was preserved in human cells. Thus, the enhanced death of activated A20-deficient T cells was caspase independent, was associated with increased formation of RIPK1-RIPK3 complexes, and required the kinase activity of RIPK1 and the expression of RIPK3.

### A20 and RIPK3 control T cell survival during *in vivo* activation

To determine whether A20 regulates the survival and responses of T cells *in vivo*, we interbred $A20^{fl}$ mice with OT-II mice, which transgenically express an ovalbumin (OVA)-specific TCR. We adoptively

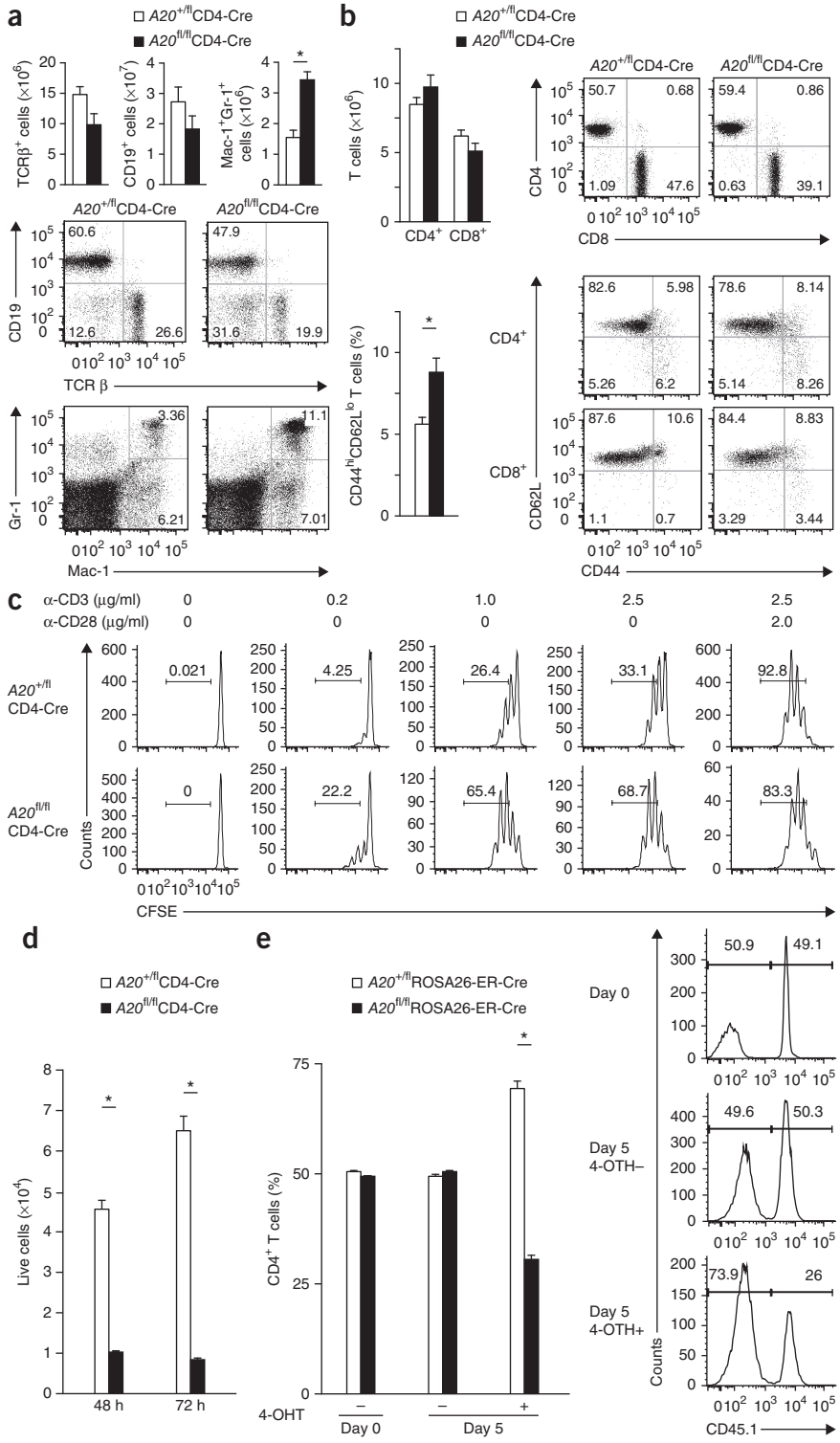


**Figure 1** A20 supports T cell population expansion. (**a**) Quantification of T cells (TCRβ$^+$), B cells (CD19$^+$) and myeloid cells (Mac-1$^+$Gr-1$^+$) (top) among splenocytes from untreated *A20*$^{+/fl}$CD4-Cre and *A20*$^{fl/fl}$CD4-Cre mice, assessed by flow cytometry (below). Numbers in quadrants (middle) indicate percent CD19$^+$TCRβ$^-$ cells (top left), CD19$^-$TCRβ$^-$ cells (bottom left) or CD19$^-$TCRβ$^+$ cells (bottom right); numbers in outlined areas (bottom) indicate percent Gr-1$^+$Mac-1$^+$ cells (top right) or Gr-1$^-$ Mac-1$^+$ cells (bottom right). (**b**) Quantification of CD4$^+$ and CD8$^+$ T cells (top left) and frequency of CD4$^+$ T cells with a CD44$^{hi}$CD62$^{lo}$ phenotype (bottom left) in the lymph nodes of untreated *A20*$^{fl/fl}$CD4-Cre and *A20*$^{+/fl}$CD4-Cre mice, assessed by flow cytometry (right). Numbers in quadrants (right) indicate percent cells in each throughout. (**c**) CFSE dilution in *A20*$^{+/fl}$CD4-Cre mice and *A20*$^{fl/fl}$CD4-Cre naive CD4$^+$ T cells stimulated *in vitro* for 3 d with various doses (above plots) of agonist anti-CD3 (α-CD3) and anti-CD28 (α-CD28), assessed by flow cytometry. Numbers above bracketed lines indicate percent cells with dilution of CFSE (divided cells). (**d**) Quantification of live naive CD4$^+$ T cells (negative for the DNA-binding dye DAPI) among *A20*$^{fl/fl}$CD4-Cre and A20$^{+/fl}$CD4-Cre CD4$^+$ T cells stimulated for 48 or 72 h *in vitro* with anti-CD3 (2.5 μg/ml) and anti-CD28 (2.0 μg/ml). (**e**) Frequency of live CD4$^+$ T cells (left) among cells purified from CD45-congenic *A20*$^{+/fl}$ROSA26-ER-Cre and *A20*$^{fl/fl}$ROSA26-ER-Cre mice, then mixed and assessed without treatment (Day 0, 4-OHT–) or treated for 5 d with vehicle (Day 5, 4-OHT–) or 4-OH-tamoxifen (Day 5, 4-OHT+) during stimulation with anti-CD3 and anti-CD28; right, CD45.1 expression on DAPI$^-$ (live) cells as at left. Numbers above bracketed lines indicate percent CD45.1$^-$ (*A20*$^{+/fl}$ROSA26-ER-Cre) cells (left) or CD45.1$^+$ (*A20*$^{fl/fl}$ROSA26-ER-Cre) cells (right). **P* < 0.05 (Student's *t*-test (**a**,**b**) or two-way analysis of variance (ANOVA) followed by Bonferroni's multiple-comparison test (**d**,**e**)). Data are representative of two to four independent experiments with one pair of mice in each (mean and s.d. of *n* = 4 (**a**,**b**), *n* = 2 (**c**,**e**) or *n* = 3 (**d**) pairs of mice (one mouse per genotype in each pair throughout).

co-transferred naive *A20*$^{+/fl}$CD4-Cre OT-II (CD45.1$^+$CD45.2$^+$) CD4$^+$ T cells and *A20*$^{fl/fl}$ CD4-Cre OT-II (CD45.1$^+$) CD4$^+$ T cells into C57BL/6 (CD45.2$^+$) recipient mice, immunized the host mice with lipopolysaccharide (LPS) plus OVA peptide (amino acids 323–339) at 24 h after transfer (day 0) and quantified splenic OT-II T cells from each donor genotype at various time points after immunization. This experimental design allowed us to assess the response of A20-deficient and A20-sufficient T cells in the same milieu of cytokines and environmental factors. Consistent with the *in vitro* data, *A20*$^{fl/fl}$CD4-Cre OT-II CD4$^+$ T cell populations expanded poorly relative to the expansion of *A20*$^{+/fl}$CD4-Cre OT-II CD4$^+$ T cell populations within the same mice, after challenge with OVA (**Fig. 3a**). This result indicated that A20 supported the population expansion of activated T cells *in vivo*.

We next assessed the susceptibility of *A20*$^{fl/fl}$CD4-Cre mice to experimental autoimmune encephalomyelitis (EAE), a model of T cell–mediated autoimmunity[32]. Following immunization with a myelin oligodendrocyte glycoprotein (MOG) peptide (amino acids 35–55) in complete Freund's adjuvant, *A20*$^{fl/fl}$CD4-Cre mice developed markedly less-severe motor neuron symptoms than those of their *A20*$^{+/fl}$CD4-Cre counterparts (**Fig. 3b**). Histological studies revealed fewer lymphoid infiltrates and greater myelin preservation in spinal cord sections from *A20*$^{fl/fl}$CD4-Cre mice than in those from

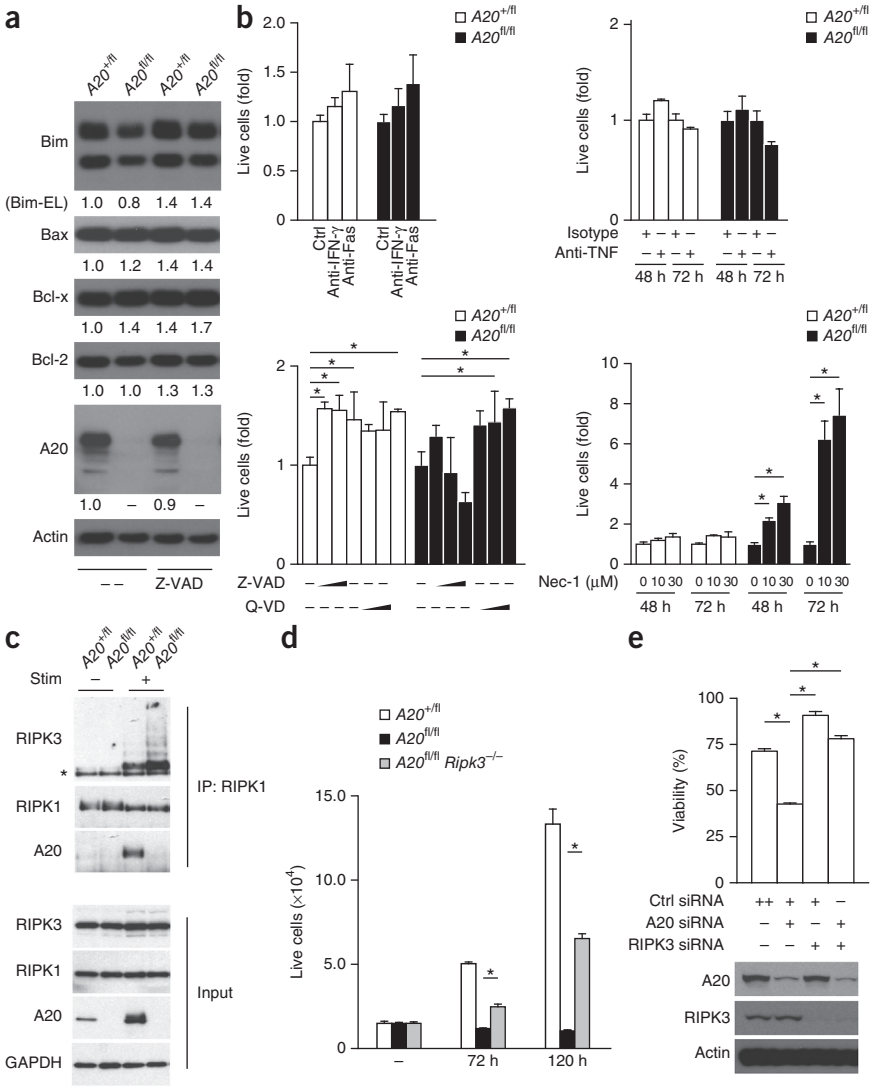


**Figure 2** A20 inhibits T cell necroptosis. (**a**) Immunoblot analyses of survival proteins (left margin), as well as actin and A20 (below; controls), in $A20^{+/fl}$CD4-Cre ($A20^{+/fl}$) and $A20^{fl/fl}$CD4-Cre ($A20^{fl/fl}$) CD4$^+$ T cells 13 h after stimulation via the TCR in the presence (Z-VAD) or absence (–) of Z-VAD. Numbers below lanes indicate quantification of density, normalized to that of actin. Bim-EL, extra-long form of Bim (top band). (**b**) Quantification of live cells among congenically marked $A20^{+/fl}$CD4-Cre and $A20^{fl/fl}$CD4-Cre T cells cultured together for 3 d with stimulation via the TCR, in the presence of inhibitory antibodies or small molecules (below plots), presented relative to results obtained in the absence (control (Ctrl) or –) of those inhibitory antibodies or small molecules. Wedges (bottom left) indicate increasing concentrations of Z-VAD (0, 10, 50 and 100 μM) or Q-VD (0, 20 and 40 μM). Isotype, Isotype-matched control antibody; Nec-1, necrostatin-1. (**c**) Immunoblot analysis of RIPK1-associated proteins in $A20^{+/fl}$CD4-Cre and $A20^{fl/fl}$CD4-Cre T cells before (–) and 8 h after (+) stimulation via the TCR with Z-VAD (Stim), assessed after immunoprecipitation (IP) with anti-RIPK1 (top) and in samples without immunoprecipitation (below (Input)). (**d**) Quantification of live $A20^{+/fl}$CD4-Cre, $A20^{fl/fl}$CD4-Cre and $A20^{fl/fl}$CD4-Cre $Ripk3^{-/-}$ ($A20^{fl/fl}Ripk3^{-/-}$) CD4$^+$ T cells before (–) and 72 or 120 h after stimulation with anti-CD3 and anti-CD28 plus Z-VAD. (**e**) Survival (top) of caspase-8 deficient Jurkat I9.2 cells transfected with various combinations of control siRNA (Ctrl siRNA) and A20- or RIPK3-specific siRNA (below graph) and stimulated 72 h later with TNF; results are presented relative to those of unstimulated Jurkat I9.2 cells. Below, immunoblot analysis of A20, RIPK3 and actin in cells as above. *$P < 0.05$ (two-way ANOVA followed by Bonferroni's multiple-comparisons test (**b**) or Tukey's test (**d**) or one-way ANOVA followed by Tukey's test (**e**)). Data are representative of three experiments with two pairs of mice in each (**a**), two experiments (**b**; error bars, s.d. of $n = 2$ pairs of mice each), three experiments (**c**) or two experiments (**e**; error bars, s.d.) or are from two experiments (**d**; error bars, s.d. of $n = 3$ sets of mice (one mouse per genotype in each set throughout)).



$A20^{+/fl}$CD4-Cre mice (**Fig. 3c**), while *ex vivo* stimulation of lymph node CD4$^+$ T cells with MOG peptide resulted in decreased proliferation of $A20^{fl/fl}$CD4-Cre T cells *in vitro* compared with that of $A20^{+/fl}$CD4-Cre T cells (**Fig. 3d**). The $T_H17$ subset of helper T cells is important in the pathogenesis of EAE[33]. We thus quantified $T_H17$ cells in the lymph nodes of mice immunized with MOG peptide and found fewer $T_H17$ cells in $A20^{fl/fl}$CD4-Cre lymph nodes than in A20$^{+/fl}$CD4-Cre lymph nodes (**Fig. 3e**), which paralleled the reduction in MOG-specific A20-deficient CD4$^+$ T cells (**Fig. 3d**). Following *in vitro* stimulation of naive CD4$^+$ T cells under conditions to polarize them into the $T_H1$ or $T_H17$ subset of helper T cells, we obtained fewer IFN-γ-producing and IL-17-producing T cells from $A20^{fl/fl}$CD4-Cre T cell cultures than from control $A20^{+/fl}$CD4-Cre T cell cultures (**Supplementary Fig. 3**), while the differentiation of $A20^{fl/fl}$CD4-Cre $Ripk3^{-/-}$ T cells into $T_H17$ or $T_H1$ cells was equal to that of $A20^{+/fl}$CD4-Cre T cells and $A20^{+/fl}$CD4-Cre $Ripk3^{-/-}$ T cells (**Supplementary Fig. 3**). Hence, T cell–specific deficiency in A20 impaired the activation of T cells and the differentiation of CD4$^+$ T cells into $T_H17$ and $T_H1$ cells and rendered mice less susceptible to EAE.

We next investigated whether RIPK3-dependent necroptosis affected the survival of A20-deficient T cells *in vivo*. RIPK3 is expressed in multiple tissues, and $Ripk3^{fl/fl}$ mice have not yet been described. Hence, we adoptively transferred CD4$^+$ T cells from $A20^{fl/fl}$CD4-Cre $Ripk3^{-/-}$, $A20^{fl/fl}$CD4-Cre $Ripk3^{+/+}$, $A20^{+/fl}$CD4-Cre $Ripk3^{-/-}$ or $A20^{+/fl}$CD4-Cre $Ripk3^{+/+}$ mice into lymphocyte-deficient $Rag1^{-/-}$ mice, which we subsequently immunized with MOG peptide. This experimental design allowed us to investigate the T cell–specific functions of A20 and RIPK3 *in vivo*. $Rag1^{-/-}$ mice that received $A20^{fl/fl}$CD4-Cre $Ripk3^{-/-}$ T cells developed more severe EAE than $Rag1^{-/-}$ mice that received $A20^{fl/fl}$CD4-Cre $Ripk3^{+/+}$ T cells (**Fig. 3f**), which suggested that abrogation of necroptosis in A20-deficient T cells restored the capacity of these T cells to cause EAE. $Rag1^{-/-}$ mice that received $A20^{+/fl}$CD4-Cre $Ripk3^{-/-}$ T cells or $A20^{+/fl}$CD4-Cre $Ripk3^{+/+}$ T cells developed more severe EAE than did mice that received A20-deficient T cells (**Fig. 3f**). Together these data indicated that A20 protected activated CD4$^+$ T cells from RIPK3-dependent necroptosis *in vivo*.

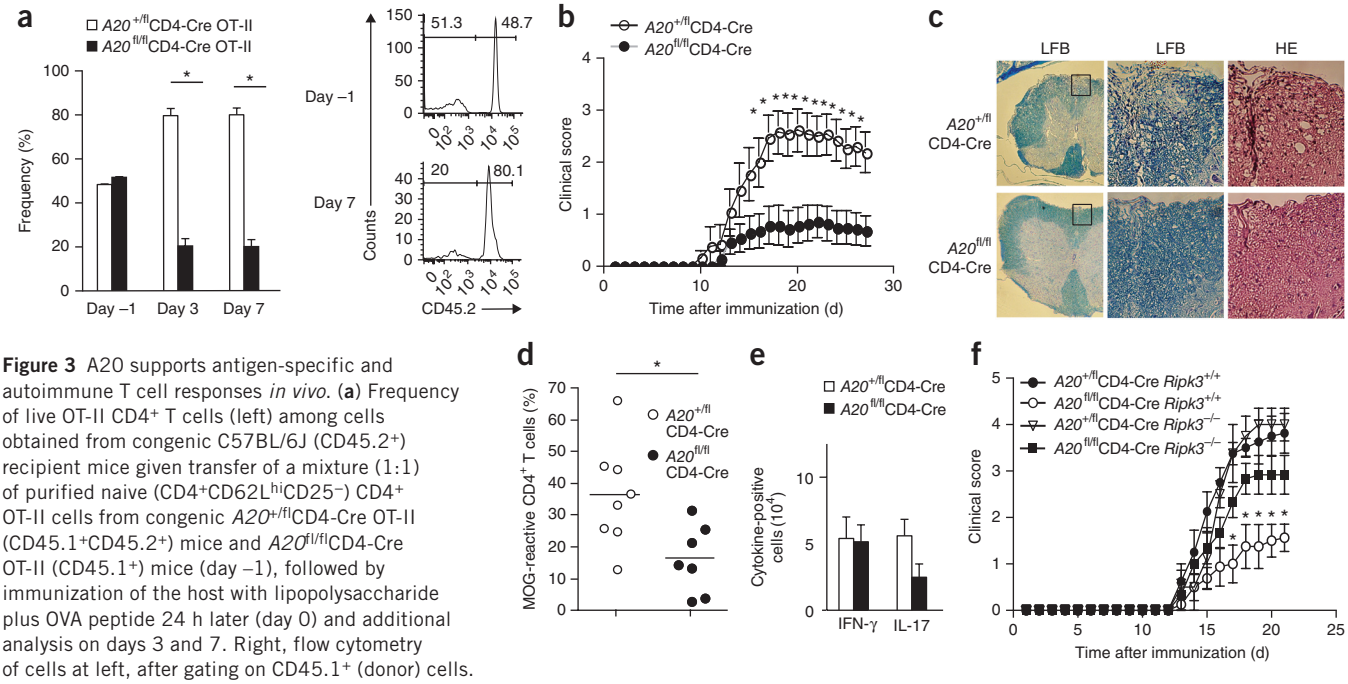


**Figure 3** A20 supports antigen-specific and autoimmune T cell responses *in vivo*. (**a**) Frequency of live OT-II CD4$^+$ T cells (left) among cells obtained from congenic C57BL/6J (CD45.2$^+$) recipient mice given transfer of a mixture (1:1) of purified naive (CD4$^+$CD62L$^{hi}$CD25$^-$) CD4$^+$ OT-II cells from congenic *A20*$^{+/fl}$CD4-Cre OT-II (CD45.1$^+$CD45.2$^+$) mice and *A20*$^{fl/fl}$CD4-Cre OT-II (CD45.1$^+$) mice (day –1), followed by immunization of the host with lipopolysaccharide plus OVA peptide 24 h later (day 0) and additional analysis on days 3 and 7. Right, flow cytometry of cells at left, after gating on CD45.1$^+$ (donor) cells. Numbers above bracketed lines indicate percent CD45.2$^-$ (*A20*$^{fl/fl}$CD4-Cre OT-II) cells (left) or CD45.2$^+$ (*A20*$^{+/fl}$CD4-Cre OT-II) cells (right) among the CD45.1$^+$ cells. (**b**) EAE clinical scores of *A20*$^{+/fl}$CD4-Cre and *A20*$^{fl/fl}$CD4-Cre mice after immunization with MOG peptide plus complete Freund's adjuvant. (**c**) Histopathological analysis of spinal cord sections from mice 30 d after immunization as in **b**, showing staining of myelin content with Luxol fast blue (LFB) (left); middle and right, enlargement of areas outlined at left, showing tissue with infiltrating lymphocytes, stained with Luxol fast blue and with hematoxylin and eosin (HE). Original magnification, ×40 (left) or ×200 (middle and right). (**d**) Quantification of MOG-reactive CD4$^+$ T cells among cells obtained from the lymph nodes of mice 9 d after immunization as in **b**, then labeled with CFSE and re-stimulated for 3 d *in vitro* with MOG peptide, assessed by flow cytometry and presented as the frequency of CFSE-labeled T cells in diluted peaks relative to those in undiluted peaks. Each symbol represents an individual mouse ($n = 8$ (*A20*$^{+/fl}$CD4-Cre) or 7 (and *A20*$^{fl/fl}$CD4-Cre)); small horizontal lines indicate the mean. (**e**) Intracellular expression of IFN-γ and IL-17 in CD4$^+$ T cells obtained from the lymph nodes of mice immunized as in **b** and re-stimulated with MOG peptide *in vitro*, quantified by flow cytometry. (**f**) EAE clinical scores of *Rag1*$^{-/-}$ mice bearing *A20*$^{+/fl}$CD4-Cre *Ripk3*$^{+/+}$, *A20*$^{fl/fl}$CD4-Cre *Ripk3*$^{+/+}$, *A20*$^{+/fl}$CD4-Cre *Ripk3*$^{-/-}$ or *A20*$^{fl/fl}$CD4-Cre *Ripk3*$^{-/-}$ T cells, assessed at various times (horizontal axis) after immunization with MOG peptide. $^*P < 0.05$ (two-way ANOVA followed by Bonferroni's multiple-comparisons test (**a**,**b**,**f**) or Student's *t*-test (**d**,**e**)). Data are from two independent experiments (**a**,**b**,**e**,**f**; error bars, mean and s.e.m. of $n = 3$ mice per genotype (**a**), $n = 14$ mice per genotype (**b**–**e**) or $n = 5$ mice per donor genotype (**f**)) or are representative of two experiments (**c**).



## A20 protects mice from RIPK3-dependent necroptosis

Necroptotic death typically triggers inflammation *in vivo* due to the release of intracellular molecules from dying cells[34]. Tissue death and inflammation are hallmarks of *A20*$^{-/-}$ mice[2]. To investigate whether A20 might prevent necroptosis in cells other than T cells, we derived mice bearing germline deletion of *A20*$^{fl/fl}$ (called '*A20*$^{KO2}$ mice' here) by interbreeding *A20*$^{fl/fl}$ mice with B6.EIIA-Cre mice (which results in deletion of *lox*P-flanked alleles in the early mouse embryo)[15]. We bred *A20*$^{KO2}$ mice to C57BL/6 mice to generate *A20*$^{KO2}$ mice lacking the EIIA-Cre transgene. We subsequently crossed *A20*$^{KO2}$ mice with *Ripk3*$^{-/-}$ mice to generate *A20*$^{KO2/KO2}$*Ripk3*$^{-/-}$ double-mutant mice (on the C57BL/6 background). While most *A20*$^{KO2/KO2}$*Ripk3*$^{+/+}$ mice died within 1 d of birth, *A20*$^{KO2/KO2}$*Ripk3*$^{-/-}$ mice survived 2–3 weeks (**Fig. 4a**). The partial rescue of *A20*$^{KO2/KO2}$ mice from death through the introduction of RIPK3 deficiency suggested that increased systemic necroptosis contributed to the perinatal death of *A20*$^{KO2/KO2}$ mice.

Because increased necroptosis of T cells was probably not the main cause of the perinatal death of *A20*$^{KO2/KO2}$ mice, we next assessed whether A20 directly restricted necroptosis in non-T cells. We isolated mouse embryonic fibroblasts (MEFs) from *A20*$^{KO2/KO2}$ and *A20*$^{+/+}$ mice and assessed their susceptibility to death in response to TNF, cycloheximide (CHX) and Z-VAD (TNF–CHX–Z-VAD), a 'cocktail' known to induce caspase-independent necroptosis. In these conditions, as assessed by a luminescent cell-viability assay, more *A20*$^{KO2/KO2}$ MEFs than *A20*$^{+/+}$ MEFs died (**Fig. 4b**). Treatment of TNF–CHX–Z-VAD–stimulated MEFs with necrostatin-1 restored the viability of *A20*$^{KO2/KO2}$ MEFs to that of *A20*$^{+/+}$ MEFs, which suggested that the caspase-independent death induced by the TNF–CHX–Z-VAD mixture was dependent on the kinase activity of RIPK1. *A20*$^{KO2/KO2}$ *Ripk3*$^{-/-}$ MEFs were more protected from TNF–CHX–Z-VAD–induced necroptosis than were *A20*$^{KO2/KO2}$ MEFs, which indicated that A20 inhibited RIPK3-dependent necroptosis of these cells. Together these results indicated that A20 protected various cell types from necroptosis and suggested that uncontrolled necroptosis contributed to the perinatal-death phenotype of *A20*$^{KO2/KO2}$ mice.

## A20 inhibits pro-necroptotic RIPK1-RIPK3 complexes

RIPK3-dependent necroptosis involves the kinase activity of RIPK1 and the RIPK3-dependent formation of RIPK1-RIPK3 complexes[29,30]. Accordingly, we assessed whether A20 restricted the formation of RIPK1-RIPK3 complexes in a cell-autonomous fashion. We immunoprecipitated RIPK1 from *A20*$^{+/+}$ and *A20*$^{KO2/KO2}$ MEFs treated with either TNF-CHX or TNF–CHX–Z-VAD and analyzed RIPK3 expression by immunoblot. Treatment with TNF–CHX–Z-VAD induced larger amounts of RIPK1-associated RIPK3 in *A20*$^{KO2/KO2}$ MEFs than in *A20*$^{+/+}$ MEFs (**Fig. 4c**). As phosphorylation of RIPK3 is required for the formation of necroptotic RIPK1-RIPK3 complexes, we assessed the phosphorylation status of RIPK3 in *A20*$^{KO2/KO2}$ MEFs[29,30].

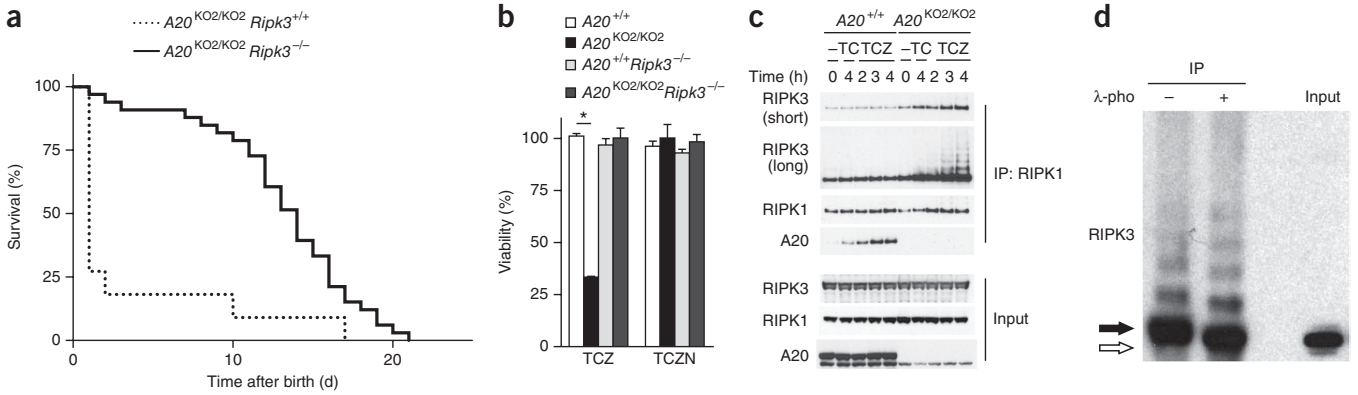


**Figure 4** A20 inhibits the formation of RIPK1-RIPK3 complexes. (**a**) Survival of $A20^{KO2/KO2}Ripk3^{-/-}$ mice ($n = 33$) and their $A20^{KO2/KO2}Ripk3^{+/+}$ littermates ($n = 16$); each 'step' represents the death of one mouse. $P < 0.0001$ (log-rank test). (**b**) Survival of $A20^{+/+}$, $A20^{KO2/KO2}$, $A20^{+/+}Ripk3^{-/-}$ and $A20^{KO2/KO2}Ripk3^{-/-}$ MEFs 4 h after stimulation with TNF–CHX–Z-VAD (TCZ) or TNF–CHX–Z-VAD and necrostatin-1 (TCZN), presented relative to live unstimulated cells of the same genotype. $^*P < 0.05$; (two-way ANOVA followed by Bonferroni's multiple-comparisons test). (**c**) Immunoblot analysis of RIPK3 (short and long exposure), RIPK1 and A20 in lysates of $A20^{+/+}$ or $A20^{KO2/KO2}$ MEFs stimulated for 0–4 h (above lanes) with TNF-CHX (TC) or TNF–CHX–Z-VAD (TCZ), assessed after immunoprecipitation with anti-RIPK1 (top) or in whole-cell lysates without immunoprecipitation (below). (**d**) Immunoblot analysis of RIPK3 in lysates of $A20^{KO2/KO2}$ MEFs stimulated as in **c**, followed by immunoprecipitation with anti-RIPK1 and treatment with λ-phosphatase (λ-pho +) or control buffer (λ-pho –) (left), and in whole-cell lysates without immunoprecipitation (far right). Filled arrow indicates phosphorylated RIPK3; open arrow indicates de-phosphorylated RIPK3. Data are representative of one experiment (**a**), four experiments (**b**; error bars, s.d.), three experiments (**c**) or two experiments (**d**).

We stimulated $A20^{KO2/KO2}$ MEFs with TNF–CHX–Z-VAD, immunoprecipitated proteins with anti-RIPK1 and then treated the immunoprecipitates with λ-phosphatase (or buffer alone, as a control), followed by immunoblot analyses of RIPK3. These experiments revealed that RIPK1-associated RIPK3 was almost completely phosphorylated (**Fig. 4d**), which suggested that A20 inhibited the formation of pro-necroptotic RIPK1-RIPK3 complexes that contained phosphorylated RIPK3.

### RIPK3 ubiquitination supports RIPK1-RIPK3 complexes

The laddered species at ~8-kilodalton intervals detected with anti-RIPK3 in the immunoprecipitates generated with anti-RIPK1 (**Fig. 4c**,**d**) suggested that the RIPK3 proteins, rather than non-covalently associated co-precipitated proteins, were modified. To more precisely define the ubiquitination of RIPK3, we used an antibody directed against glycine-glycine (di-glycine) linked to the ε-amino side chain of lysine, the peptide remnant of trypsinized lysates of ubiquitinated proteins[35]. This antibody allows enrichment of ubiquitinated peptides from trypsinized lysates and can be coupled with liquid chromatography–mass spectrometry to precisely identify ubiquitinated lysines in cell lysates. We used this approach to identify ubiquitinated RIPK3 peptides in necroptotic MEFs. We stimulated $A20^{KO2/KO2}$ MEFs with TNF–CHX–Z-VAD, prepared lysates after 3 h, trypsinized the whole-cell lysates, immunoprecipitated ubiquitinated peptides with the antibody to di-glycine and performed mass spectrometry on the affinity-purified ubiquitinated peptides. Tandem mass spectra from $A20^{KO2/KO2}$ MEF lysates repeatedly revealed a precursor ion with a mass/charge ($m/z$) value of $1006.0525^{+2}$ (**Fig. 5a**). A database search identified this species as a peptide spanning the amino acids at positions 2–19 of RIPK3, which was acetylated at the amino terminus and carried a di-glycine remnant at Lys5 (K5) (theoretical monoisotopic $m/z$ value of $1006.0522^{+2}$). Because we observed this modification of endogenous proteins from TNF–CHX–Z-VAD–stimulated $A20^{KO2/KO2}$ MEFs, these observations indicated that RIPK3 ubiquitination at K5 was a physiological modification.

To determine if the ubiquitination of RIPK3 at K5 was dependent on A20, we performed stable isotope labeling of $A20^{KO2/KO2}$ and wild-type ($A20^{+/+}$) MEFs[35]. We cultured $A20^{KO2/KO2}$ MEFs for 2 weeks in medium containing amino acids labeled with a light (normal) isotope and cultured $A20^{+/+}$ MEFs for 2 weeks in medium containing amino acids labeled with a heavy isotope. We confirmed by mass spectrometry the complete replacement of endogenous amino acids by isotope-labeled residues (data not shown). We then stimulated the labeled MEFs for 3 h with TNF–CHX–Z-VAD, mixed lysates from $A20^{KO2/KO2}$ and $A20^{+/+}$ MEFs, trypsinized the combined lysates, immunoprecipitated ubiquitinated peptides and analyzed the products by liquid chromatography–mass spectrometry. Tandem mass spectra revealed peptide species with an $m/z$ of ~1006 (**Fig. 5b**), which indicated the presence of RIPK3 peptide ubiquitinated at K5 in $A20^{KO2/KO2}$ MEFs with normal ('light') isotope labeling. These spectra also revealed species at an $m/z$ of ~1015 (**Fig. 5b**, left), indicative of RIPK3 peptide modified at K5 with heavy isotope–labeled residues in $A20^{+/+}$ MEFs. Direct comparison of the relative intensity of these peaks showed that species with an $m/z$ of ~1006 were ~15-fold more abundant than species with an $m/z$ of ~1015 (**Fig. 5b**, right), which indicated that $A20^{KO2/KO2}$ MEFs contained 15-fold greater amounts of K5-ubiquitinated RIPK3 peptide than did $A20^{+/+}$ MEFs. As $A20^{KO2/KO2}$ MEFs expressed amounts of total RIPK3 protein similar to those expressed by $A20^{+/+}$ MEFs (**Fig. 4c**), these findings indicated that the proportion as well as the total amount of RIPK3 protein that was ubiquitinated at K5 was much greater in A20-deficient cells. We did not detect K5-ubiquitinated RIPK3 peptides in lysates of unstimulated $A20^{KO2KO2}$ or $A20^{+/+}$ MEFs (data not shown), which supported the notion that ubiquitination of RIPK3 at K5 was induced during necroptosis.

To determine the functional importance of the ubiquitination of RIPK3 at K5 in necroptosis, we substituted the lysine at position 5 with alanine (RIPK3(K5A)) or arginine (RIPK3(K5R)). Because the RIPK3(K5R) mutant was not stable (data not shown), we assessed the ability of RIPK3(K5A) to form RIPK1-RIPK3 complexes in necroptotic cells. We virally transduced $A20^{KO2/KO2}Ripk3^{-/-}$ MEFs to express wild-type RIPK3 or RIPK3(K5A), sorted transduced cells expressing similar amounts of RIPK3 and analyzed the expression of RIPK1-associated RIPK3 as well as the amount of cellular necroptosis following stimulation with TNF–CHX–Z-VAD. MEFs expressing

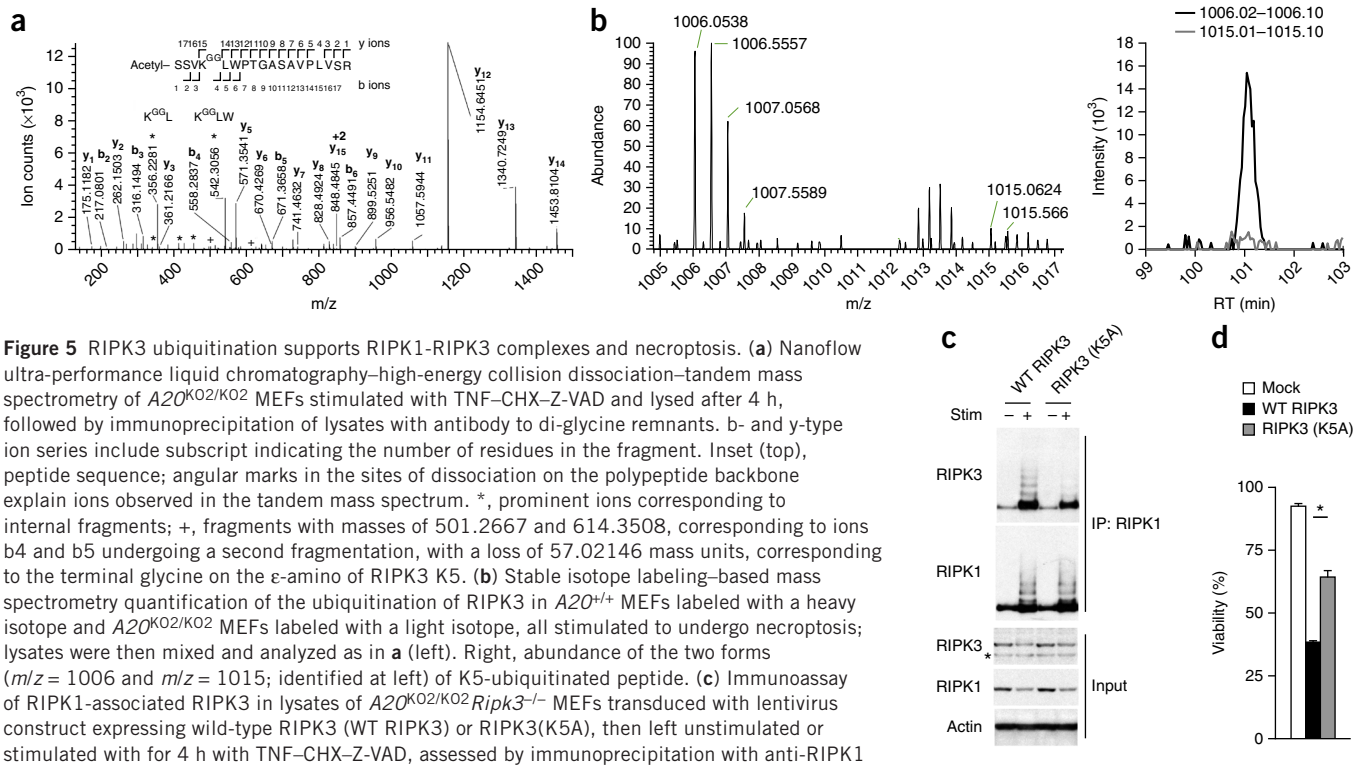


**Figure 5** RIPK3 ubiquitination supports RIPK1-RIPK3 complexes and necroptosis. (**a**) Nanoflow ultra-performance liquid chromatography–high-energy collision dissociation–tandem mass spectrometry of *A20*$^{KO2/KO2}$ MEFs stimulated with TNF–CHX–Z-VAD and lysed after 4 h, followed by immunoprecipitation of lysates with antibody to di-glycine remnants. b- and y-type ion series include subscript indicating the number of residues in the fragment. Inset (top), peptide sequence; angular marks in the sites of dissociation on the polypeptide backbone explain ions observed in the tandem mass spectrum. *, prominent ions corresponding to internal fragments; +, fragments with masses of 501.2667 and 614.3508, corresponding to ions b4 and b5 undergoing a second fragmentation, with a loss of 57.02146 mass units, corresponding to the terminal glycine on the ε-amino of RIPK3 K5. (**b**) Stable isotope labeling–based mass spectrometry quantification of the ubiquitination of RIPK3 in *A20*$^{+/+}$ MEFs labeled with a heavy isotope and *A20*$^{KO2/KO2}$ MEFs labeled with a light isotope, all stimulated to undergo necroptosis; lysates were then mixed and analyzed as in **a** (left). Right, abundance of the two forms ($m/z$ = 1006 and $m/z$ = 1015; identified at left) of K5-ubiquitinated peptide. (**c**) Immunoassay of RIPK1-associated RIPK3 in lysates of *A20*$^{KO2/KO2}$*Ripk3*$^{-/-}$ MEFs transduced with lentivirus construct expressing wild-type RIPK3 (WT RIPK3) or RIPK3(K5A), then left unstimulated or stimulated with for 4 h with TNF–CHX–Z-VAD, assessed by immunoprecipitation with anti-RIPK1 and immunoblot analysis of RIPK3 (top) or RIPK1 (middle). Below (Input), immunoblot analysis of RIPK3, RIPK1 and actin in whole-cell lysates without immunoprecipitation; *, nonspecific band below the specific RIPK3 band. (**d**) Viability of *A20*$^{KO2/KO2}$*Ripk3*$^{-/-}$ MEFs mock-transduced or transduced and stimulated as in **c**, presented relative to that of unstimulated cells. *$P < 0.05$ (one-way ANOVA followed by Tukey's test). Data are representative of three experiments (error bars (**d**), s.d.).



RIPK3(K5A) had fewer RIPK1-RIPK3 complexes than did cells expressing wild-type RIPK3 (**Fig. 5c**). Furthermore, cells expressing RIPK3(K5A) survived significantly better than did cells expressing wild-type RIPK3 (**Fig. 5d**), which indicated that ubiquitination of RIPK3 at K5 supported the formation of RIPK1-RIPK3 complexes and necroptosis.

### A20 uses its deubiquitinating motif to restrict necroptosis

Polyubiquitin chains of various conformations are added to target proteins during cell signaling[18]. Because A20 restricts the ubiquitination of RIPK1 with K63-linked polyubiquitin chains[3,4,19], we investigated whether A20 also inhibits the ubiquitination of RIPK3 with K63-linked polyubiquitin chains. We transfected 293T human embryonic kidney cells with plasmids expressing RIPK3 and hemagglutinin-tagged ubiquitin in which all lysine residues except the lysine at position 63 (K63) were replaced. We immunoprecipitated proteins from cell lysates with anti-RIPK3 and analyzed the immunoprecipitates by immunoblot with anti-hemagglutinin to reveal a ladder of K63-ubiqitinated RIPK3 (**Fig. 6a**). The addition of increasing amounts of plasmid encoding Flag-tagged A20 to the transfection led to a progressive decrease in the amount of signal from the hemagglutinin-tagged ubiquitin with replacement of all lysine residues except K63 (**Fig. 6a**), which indicated that A20 inhibited the K63-linked ubiquitination of RIPK3 in a dose-dependent fashion. In addition, following stimulation with TNF–CHX–Z-VAD, we found more K63-linked ubiquitination of RIPK3 in *A20*$^{KO2/KO2}$ MEFs than in *A20*$^{+/+}$ MEFs (**Fig. 6b**). Thus, A20 restricted the K63-linked ubiquitination of RIPK3.

To determine the mechanism by which A20 restricted the ubiquitination of RIPK3, we used MEFs from two lines of mice bearing knock-in point mutations of the gene encoding A20 that abrogate the enzymatic activity of each domain of A20. *A20*$^{OTU}$ mice bear a mutation in sequence encoding the catalytic Cys103 residue of A20 that mediates its deubiquitinating activity[19]. *A20*$^{ZF4}$ mice bear point mutations in sequence encoding residues Cys609 and Cys612 in the ZF4 motif that mediates the binding of A20 to ubiquitinated RIPK1 and E2 enzymes[19,22]. *A20*$^{ZF4/ZF4}$ and wild-type (*A20*$^{+/+}$) MEFs showed similar viability in response to TNF–CHX–Z-VAD, whereas *A20*$^{OTU/OTU}$ MEFs had reduced viability (**Fig. 6c**), which indicated that A20 used its catalytic deubiquitinating Cys103 residue to inhibit necroptosis.

To understand how the Cys103 and ZF4 motifs of A20 regulate necroptotic signaling complexes, we analyzed the formation of RIPK1-RIPK3 complexes in *A20*$^{ZF4ZF4}$ and *A20*$^{OTUOTU}$ MEFs. After stimulating *A20*$^{+/+}$, *A20*$^{ZF4ZF4}$ and *A20*$^{OTUOTU}$ MEFs for 3 or 4 h with TNF–CHX–Z-VAD, we immunoprecipitated proteins from cell lysates with anti-RIPK1 and analyzed the immunoprecipitates by immunoblot with anti-RIPK3. *A20*$^{OTU/OTU}$ MEFs contained considerably more RIPK1-RIPK3 complexes than did *A20*$^{+/+}$ or *A20*$^{ZF4/ZF4}$ MEFs (**Fig. 6d**), while *A20*$^{ZF4/ZF4}$ MEFs contained slightly more RIPK1-RIPK3 complexes than did *A20*$^{+/+}$ or *A20*$^{+/+}$ MEFs (**Fig. 6d**). RIPK1-associated RIPK3 showed a laddered pattern indicative of ubiquitination in *A20*$^{OTU/OTU}$ MEFs (**Fig. 6d**). Following stimulation via the TCR, *A20*$^{OTU/-}$ T cells also had more RIPK1-RIPK3 association and greater ubiquitination of RIPK3 than either *A20*$^{ZF4/-}$ T cells or *A20*$^{+/-}$ T cells had (**Fig. 6e**), which indicated that Cys103 regulated the ubiquitination of RIPK3 and the formation of RIPK1-RIPK3 complexes in T cells as well as in MEFs. *A20*$^{OTU/OTU}$ and *A20*$^{ZF4/ZF4}$ T cells stimulated via the TCR and also stimulated with Z-VAD exhibited phenotypes similar to those of *A20*$^{OTU/-}$ and

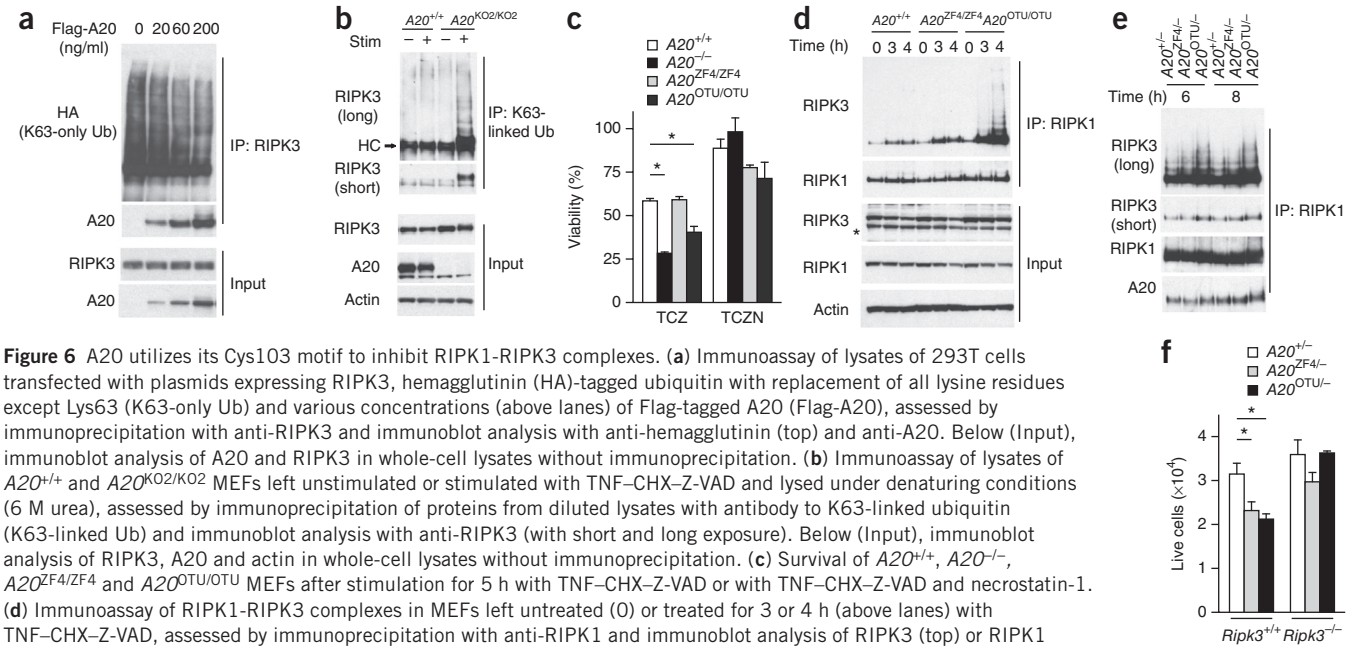


**Figure 6** A20 utilizes its Cys103 motif to inhibit RIPK1-RIPK3 complexes. (**a**) Immunoassay of lysates of 293T cells transfected with plasmids expressing RIPK3, hemagglutinin (HA)-tagged ubiquitin with replacement of all lysine residues except Lys63 (K63-only Ub) and various concentrations (above lanes) of Flag-tagged A20 (Flag-A20), assessed by immunoprecipitation with anti-RIPK3 and immunoblot analysis with anti-hemagglutinin (top) and anti-A20. Below (Input), immunoblot analysis of A20 and RIPK3 in whole-cell lysates without immunoprecipitation. (**b**) Immunoassay of lysates of $A20^{+/+}$ and $A20^{KO2/KO2}$ MEFs left unstimulated or stimulated with TNF–CHX–Z-VAD and lysed under denaturing conditions (6 M urea), assessed by immunoprecipitation of proteins from diluted lysates with antibody to K63-linked ubiquitin (K63-linked Ub) and immunoblot analysis with anti-RIPK3 (with short and long exposure). Below (Input), immunoblot analysis of RIPK3, A20 and actin in whole-cell lysates without immunoprecipitation. (**c**) Survival of $A20^{+/+}$, $A20^{-/-}$, $A20^{ZF4/ZF4}$ and $A20^{OTU/OTU}$ MEFs after stimulation for 5 h with TNF–CHX–Z-VAD or with TNF–CHX–Z-VAD and necrostatin-1. (**d**) Immunoassay of RIPK1-RIPK3 complexes in MEFs left untreated (0) or treated for 3 or 4 h (above lanes) with TNF–CHX–Z-VAD, assessed by immunoprecipitation with anti-RIPK1 and immunoblot analysis of RIPK3 (top) or RIPK1 (below). Below, immunoblot analysis without immunoprecipitation (as in **Fig. 5c**). (**e**) Immunoassay of RIPK1-RIPK3 complexes in $A20^{+/-}$, $A20^{ZF4/-}$ and $A20^{OTU/-}$ T cells stimulated for 6 or 8 h (above lanes) with anti-CD3, anti-CD28 and Z-VAD, assessed by immunoblot analysis of RIPK3 (top; short and long exposure), RIPK1 (below) and A20 (bottom). (**f**) Quantification of live RIPK3-sufficient ($Ripk3^{+/+}$) or RIPK3-deficient ($Ripk3^{-/-}$) (horizontal axis) $A20^{+/-}$, $A20^{ZF4/-}$ and $A20^{OTU/-}$ T cells (key) after stimulation for 72 h as in **e**. $^*P < 0.05$, compared with wild-type cells (two-way ANOVA followed by Bonferroni's multiple-comparisons test). Data are representative of three independent experiments (error bars (**c**,**f**), s.d.).

$A20^{ZF4/-}$ T cells stimulated similarly (data not shown). In addition, following 72 h of stimulation with anti-CD3, anti-CD28 and Z-VAD, the survival of RIPK3-sufficient ($Ripk3^{+/+}$) $A20^{OTU/-}$ and $A20^{ZF4/-}$ T cells was decreased compared with that of their $A20^{+/-}$ counterparts (**Fig. 6f**). Finally, we crossed $A20^{OTU}$ and $A20^{ZF4}$ mice with $Ripk3^{-/-}$ mice, isolated naive CD4$^+$ T cells from the progeny of those crosses and assessed the response of the cells to stimulation via the TCR plus stimulation with Z-VAD. Following such stimulation for 72 h, the population expansion of $A20^{OTU/-}Ripk3^{-/-}$ CD4$^+$ T cells was the same as that of $A20^{+/-}$ $Ripk3^{-/-}$ T cells, and the population expansion of $A20^{ZF4/-}Ripk3^{-/-}$ CD4$^+$ T cells was partially restored to that of $A20^{+/-}$ T cells (**Fig. 6f**), which indicated that RIPK3 deficiency restored the population expansion of $A20^{OTU/-}$ CD4$^+$ T cells and, to a lesser extent, $A20^{ZF4/-}$ CD4$^+$ T cells after such stimulation. This indicated that while the ZF4 motif of A20 was required for normal A20 activity during T cell activation, the Cys103-dependent deubiquitination function of A20 was needed to inhibit the formation of RIPK1-RIPK3 complexes and RIPK3-dependent necroptosis.

## DISCUSSION

Our study has revealed that A20 restricted necroptosis in multiple cell types. These findings suggest that A20 regulates cellular and tissue homeostasis as well as immunological homeostasis. We discovered that RIPK3 underwent a specific ubiquitination event that supported the formation of RIPK1-RIPK3 complexes in cells undergoing necroptosis, and that A20 potently inhibited this event. Our studies have broad implications for the molecular regulation of cell-death signaling as well as the physiological mechanisms by which A20 prevents inflammatory diseases.

We found that uncontrolled RIPK3-dependent necroptosis in the absence of A20 inhibited T cell population expansion *in vitro* and *in vivo*. Exaggerated necroptosis in caspase-8-deficient T cells and T cells expressing mutant FADD has been reported to compromise anti–lymphocytic choriomeningitis virus or anti-toxoplasma responses[27,28]. Hence, our studies reinforce the concept that in certain pathological contexts, necroptosis can restrict the population expansion of activated T cells. Our studies also indicated dual roles for A20 in T cells, restricting both cellular activation and cell death. Activation and survival signals appear to be integrated differently in activated T cells than in activated B cells, in which A20 deficiency causes increased NF-κB-dependent expression of Bcl-x and resistance to Fas-mediated death[13]. These differences reemphasize the importance of studying the cell type–specific functions of pleiotropically expressed molecules to understand their physiological roles in disease pathogenesis.

Our finding that $A20^{KO2/KO2}Ripk3^{-/-}$ mice lived longer than $A20^{KO2/KO2}Ripk3^{+/+}$ mice suggested that A20 protects multiple cell types from necroptosis. Thus, loss of A20 from other cells (for example, stromal cells) might render mice more susceptible to necroptotic tissue damage. Our observations are consistent with published experiments showing that A20 protects L929 mouse fibrosarcoma cells from TNF-induced death[36]. RIPK3 deficiency might also abrogate inflammasome activity in $A20^{-/-}$ mice[37]. Because A20 also protects cells from apoptotic death[2,38], the anti-necroptotic function of A20 positions this molecule as a potent pro-survival protein. The idea that necroptosis of target organs might contribute to disease severity in inflammatory bowel disease and other conditions has been suggested[39]. Given our findings, together with observations that polymorphisms of A20 are associated with more-severe nephritic complications of patients with systemic lupus erythematosus[40] and increased disease severity in patients with psoriasis vulgaris[41] or cystic fibrosis[42], we propose that A20 might partly prevent human disease by protecting against necroptotic death in non-lymphoid tissues.

Necroptosis is known to occur in cells lacking pro-apoptotic molecules such as caspase-8 and FADD[43–46]. This has been explained by the cleavage of RIPK1 by caspase-8, which prevents RIPK1-dependent

formation of RIPK1-RIPK3 complexes. Virus-infected cells may also undergo necroptosis when viral proteins abrogate apoptosis[30]. Hence, necroptosis has been viewed as a form of cell death that occurs predominantly in cells rendered caspase deficient. In contrast, we found that A20-deficient MEFs exhibited increased sensitivity to both apoptosis and necroptosis[2]. Therefore, our findings suggest that A20 restricts necroptosis by a mechanism that is distinct from that used by caspase-8 or FADD.

The ubiquitination of RIPK1 inhibits its kinase activity, and the deubiquitinating enzyme CylD supports necroptosis by deubiquitinating RIPK1 (refs. 46,47). Like CylD, A20 inhibits RIPK1 ubiquitination and NF-κB signaling[3,19]. However, our findings have shown that unlike CylD, A20 inhibited necroptosis. This divergence suggests that A20 inhibits necroptosis via a mechanism other than inhibiting the ubiquitination of RIPK1. Our finding that A20 restricted the ubiquitination of RIPK3 provides such a mechanism. K63-linked ubiquitination of RIPK1 and RIPK2 occurs during NF-κB signaling induced by TNF and Nod2, respectively, and *A20*$^{-/-}$ MEFs and *A20*$^{-/-}$ macrophages exhibit increased ubiquitination of RIPK1 and RIPK2, respectively, when stimulated through these pathways[3,10,19]. Hence, A20 seems to restrict the ubiquitination of RIPK1, RIPK2 and RIPK3 in distinct signaling contexts. The E3 ligases of the cIAP family are able to ubiquitinate proteins of the RIPK family *in vitro*, and cIAP1 and cIAP2 may be responsible for activating RIPK1 and RIPK2 by supporting their ubiquitination with K63-linked chains following activation of the TNF and Nod2 pathway[48,49]. Hence, cIAP proteins might similarly activate RIPK3 through ubiquitination during necroptosis. However, cIAP proteins seem to limit necroptosis in macrophages[50]. Thus, if cIAP proteins activate RIPK3 and support the formation of RIPK1-RIPK3 complexes and necroptosis, they probably also perform a separate function that restricts necroptosis (for example, cIAP proteins might ubiquitinate RIPK1). Future studies will be needed to identify the physiological E3 ligases that ubiquitinate RIPK3.

Our mass spectrometry screen identified K5 of RIPK3 as a physiological ubiquitination site, and our stable-isotope-labeling experiments revealed that *A20*$^{-/-}$ MEFs contained 15-fold more RIPK3 peptide ubiquitinated at K5 than *A20*$^{+/+}$ MEFs had. Substitution of this residue abrogated the ubiquitination of RIPK3 and the formation of RIPK1-RIPK3 complexes and necroptosis. In other signaling complexes, K63-linked ubiquitination facilitates the recruitment of K63-ubiquitin sensor proteins[18]. Hence, K63-linked ubiquitination of RIPK3 could similarly support the recruitment of other ubiquitin sensors. These ubiquitin-binding proteins could in turn enhance the kinase activity of RIPK3, support RIPK1-RIPK3 complexes, recruit downstream mediators such as MLKL[51], and/or support higher-order amyloid complexes composed of RIPK1 and RIPK3 proteins[31]. Structurally, K5 resides in an unstructured portion of RIPK3 and is thus probably accessible for ubiquitination[52]. In addition, the K5 residue is conserved in human RIPK3, and RIPK3 deficiency abrogated the increased necroptosis of A20-deficient human Jurkat I9.2 T cells. Thus, ubiquitination of RIPK3 may support necroptosis in human cells. Therefore, ubiquitination can support necroptosis, and A20 substantially inhibits this pro-necroptotic ubiquitination event.

We found that the Cys103 deubiquitinating motif of A20 was required for inhibition of the ubiquitination of RIPK3 and formation of RIPK1-RIPK3 complexes. The Cys103 motif cleaves unanchored K48 ubiquitin chains as well as RIPK1- or TRAF6-anchored K63 chains in cell-free experiments[3,4,20]. This motif has also been shown to inhibit E2-E3 interactions in cells[21]. Both of these Cys103-dependent activities could inhibit the K63-linked polyubiquitination of RIPK3. In contrast, the ZF4 domain of A20, which binds ubiquitin and supports E3 ligase activity, appeared to be less critical than Cys103 in inhibiting the ubiquitination of RIPK3 during necroptosis. One possible explanation for this difference could be that A20, which relies on ZF4 to bind ubiquitinated RIPK1, may rely more on other ubiquitin-binding motifs, such as ZF7, to bind ubiquitinated RIPK3. Such distinct roles for the biochemical motifs of A20 might provide important insight into how A20 performs its physiological functions.

In conclusion, we have discovered that A20 restricted RIPK3 dependent necroptosis. Our studies showed that RIPK3 was physiologically ubiquitinated at K5 during necroptosis in a manner that supported the formation of RIPK1-RIPK3 complexes. The regulation of necroptosis by A20 should be integrated with the previously described roles of A20 in restricting NF-κB signaling and cellular activation. As hypomorphic A20 expression and function are linked to a wide range of human inflammatory and autoimmune diseases, and as necroptosis can trigger inflammation, our studies suggest an additional pathway by which A20 prevents human disease.

## METHODS

Methods and any associated references are available in the online version of the paper.

*Note: Any Supplementary Information and Source Data files are available in the online version of the paper.*

### ACKNOWLEDGMENTS

We thank X. Wang for *Ripk3*$^{-/-}$ mice; J.C. Patarroyo and N. Molnarfi for assistance with EAE experiments; and S. Oakes for discussions. Mass spectrometry analysis was provided by the Bio-Organic Biomedical Mass Spectrometry Resource at the University of California, San Francisco, supported by funding from the Biomedical Technology Research Centers program of the National Institute of General Medical Sciences of the US National Institutes of Health (8P41GM103481) and the Howard Hughes Medical Institute. Supported by the US National Institutes of Health (DK071939 and DK095693 (A.M.), and AI073737 and NS063008 (S.S.Z.)), the Kenneth Rainin Foundation (A.M.), the National Multiple Sclerosis Society (RG 4768 and RG 5180 (S.S.Z.); and U.S.), the Guthy Jackson Charitable Foundation (S.S.Z.), the Maisin Foundation (S.S.Z.) and The Crohn's and Colitis Foundation of America (M.O. and S.O.).

### AUTHOR CONTRIBUTIONS

M.O. performed necroptosis experiments and assisted with the manuscript; S.O. performed most of the T cell studies and assisted with the manuscript; U.S.-T. designed and performed most of the EAE experiments; J.O.-P. designed and performed mass spectrometry studies; T.L. performed initial experiments of necroptosis in MEFs; R.T. and M.I.W. performed initial T cell studies; T.P. performed EAE experiments; B.D. provided mice and cell lines for necroptosis experiments; R.A. assisted with breeding and mouse experiments; A.A. and J.B. provided technical assistance; H.W. analyzed RIPK3 structure; A.B. supervised mass spectrometry studies; B.A.M. supervised T cell and necroptosis studies and helped write the manuscript; S.S.Z. supervised EAE experiments; and A.M. supervised the overall study and wrote the manuscript.

### COMPETING FINANCIAL INTERESTS

The authors declare no competing financial interests.



1. Opipari, A.W. Jr., Boguski, M.S. & Dixit, V.M. The A20 cDNA induced by tumor necrosis factor alpha encodes a novel type of zinc finger protein. *J. Biol. Chem.* **265**, 14705–14708 (1990).
2. Lee, E.G. *et al.* Failure to regulate TNF-induced NF-κB and cell death responses in A20-deficient mice. *Science* **289**, 2350–2354 (2000).
3. Wertz, I.E. *et al.* De-ubiquitination and ubiquitin ligase domains of A20 downregulate NF-κB signalling. *Nature* **430**, 694–699 (2004).
4. Boone, D.L. *et al.* The ubiquitin modifiying enzyme A20 is essential for terminating TLR signaling. *Nat. Immunol.* **5**, 1052–1060 (2004).
5. Ma, A. & Malynn, B.A. A20: linking ubiquitination with immunity and human diseases. *Nat. Rev. Immunol.* **12**, 774–785 (2012).

6. Catrysse, L., Vereecke, L., Beyaert, R. & van Loo, G. A20 in inflammation and autoimmunity. *Trends Immunol.* **35**, 22–31 (2014).
7. Musone, S. *et al.* Multiple polymorphisms in the TNFAIP3 region are independently associated with systemic lupus erythematosus. *Nat. Genet.* **40**, 1062–1064 (2008).
8. Adrianto, I. *et al.* Association of a functional variant downstream of TNFAIP3 with systemic lupus erythematosus. *Nat. Genet.* **43**, 253–258 (2011).
9. Turer, E.E. *et al.* Homeostatic MyD88-dependent signals cause lethal inflammation in the absence of A20. *J. Exp. Med.* **205**, 451–464 (2008).
10. Hitotsumatsu, O. *et al.* The ubiquitin-editing enzyme A20 restricts nucleotide-binding oligomerization domain containing 2-triggered signals. *Immunity* **28**, 381–390 (2008).
11. Kool, M. *et al.* The ubiquitin-editing protein A20 prevents dendritic cell activation, recognition of apoptotic cells, and systemic autoimmunity. *Immunity* **35**, 82–96 (2011).
12. Hammer, G.E. *et al.* Expression of A20 by dendritic cells preserves immune homeostasis and prevents colitis and spondyloarthritis. *Nat. Immunol.* **12**, 1184–1193 (2011).
13. Matmati, M. *et al.* A20 (TNFAIP3) deficiency in myeloid cells triggers erosive polyarthritis resembling rheumatoid arthritis. *Nat. Genet.* **43**, 908–912 (2011).
14. Heger, K. *et al.* A20 deficient mast cells exacerbate inflammatory responses in vivo. *PLoS Biol.* **12**, e1001762 (2014).
15. Tavares, R.M. *et al.* The ubiquitin modifying enzyme A20 restricts B cell survival and prevents autoimmunity. *Immunity* **33**, 181–191 (2010).
16. Chu, Y. *et al.* B cells lacking the tumor suppressor TNFAIP3/A20 display impaired differentiation and hyperactivation and cause inflammation and autoimmunity in aged mice. *Blood* **117**, 2227–2236 (2011).
17. Hövelmeyer, N. *et al.* A20 deficiency in B cells enhances B-cell proliferation and results in the development of autoantibodies. *Eur. J. Immunol.* **41**, 595–601 (2011).
18. Chen, Z.J. & Sun, L. J Nonproteolytic functions of ubiquitin in cell signaling. *Mol. Cell* **33**, 275–286 (2009).
19. Lu, T.T. *et al.* Dimerization and ubiquitin mediated recruitment of A20, a complex deubiquitinating enzyme. *Immunity* **38**, 896–905 (2013).
20. Lin, S.C. *et al.* Molecular basis for the unique deubiquitinating activity of the NF-κB inhibitor A20. *J. Mol. Biol.* **376**, 526–540 (2008).
21. Shembade, N., Ma, A. & Harhaj, E.W. Inhibition of NF-κB signaling by A20 through disruption of ubiquitin enzyme complexes. *Science* **327**, 1135–1139 (2010).
22. Bosanac, I. *et al.* Ubiquitin binding to A20 ZnF4 is required for modulation of NF-κB signaling. *Mol. Cell* **40**, 548–557 (2010).
23. Skaug, B. *et al.* Direct, noncatalytic mechanism of IKK inhibition by A20. *Mol. Cell* **44**, 559–571 (2011).
24. Tokunaga, F. *et al.* Specific recognition of linear polyubiquitin by A20 zinc finger 7 is involved in NF-κB regulation. *EMBO J.* **31**, 3856–3870 (2012).
25. Verhelst, K. *et al.* A20 inhibits LUBAC-mediated NF-kB activation by linear polyubiquitin chains via its zinc finger 7. *EMBO J.* **31**, 3845–3855 (2012).
26. Beyaert, R., Heyninck, K. & Van Huffel, S. A20 and A20 binding proteins as cellular inhibitors of NF-κB dependent gene expression and apoptosis. *Biochem. Pharmacol.* **60**, 1143–1151 (2000).
27. Ch'en, I.L., Tsau, J.S., Molkentin, J.D., Komatsu, M. & Hedrick, S.M. Mechanisms of necroptosis in T cells. *J. Exp. Med.* **208**, 633–641 (2011).
28. Osborn, S.L. *et al.* Fas-associated death domain (FADD) is a negative regulator of T-cell receptor mediated necroptosis. *Proc. Natl. Acad. Sci. USA* **107**, 13034–13039 (2010).
29. He, S. *et al.* Receptor interacting protein kinase 3 determines cellular necroptotic responses to TNFa. *Cell* **137**, 1100–1111 (2009).
30. Cho, Y. *et al.* Phosphorylation-driven assembly of the RIPK1-RIPK3 complex regulates programmed necrosis and virus-induced inflammation. *Cell* **137**, 1112–1123 (2009).
31. Li, J. *et al.* The RIP1/RIP3 necrosome forms a functional amyloid signaling complex required for programmed necrosis. *Cell* **150**, 339–350 (2012).
32. Zamvil, S.S. & Steinman, L. The T lymphocyte in experimental allergic encephalomyelitis. *Annu. Rev. Immunol.* **8**, 579–621 (1990).
33. Cua, D.J. *et al.* Interleukin-23 rather than interleukin-12 is the critical cytokine for autoimmune inflammation of the brain. *Nature* **421**, 744–748 (2003).
34. Linkermann, A. & Green, D.R. Necroptosis. *N. Engl. J. Med.* **370**, 455–465 (2014).
35. Udeshi, N.D., Mertins, P., Svinkina, T. & Carr, S.A. Large-scale identification of ubiquitination sites by mass spectrometry. *Nat. Protoc.* **8**, 1950–1960 (2013).
36. Vanlangenakker, N. *et al.* TNF-induced necroptosis in L929 cells is tightly regulated by multiple TNFR1 complex I and II members. *Cell Death Dis.* **2**, e230 (2011).
37. Duong, B. *et al.* A20 restricts ubiquitination of pro-interleukin-1β protein complexes and suppresses NLRP3 inflammasome activity. *Immunity* **42**, 55–67 (2015).
38. Opipari, A.W., Hu, H.M., Yabkowitz, R. & Dixit, V.M. The A20 zinc finger protein protects cells from tumor necrosis factor cytotoxicity. *J. Biol. Chem.* **267**, 12424–12427 (1992).
39. Welz, P.S. *et al.* FADD prevents RIPK3-mediated epithelial cell necrosis and chronic intestinal inflammation. *Nature* **477**, 330–334 (2011).
40. Bates, J.S. *et al.* Meta-analysis and imputation identifies a 109 kb risk haplotype spanning TNFAIP3 associated with lupus nephritis and hematologic manifestations. *Genes Immun.* **10**, 470–477 (2009).
41. Jiang, X. *et al.* Expression of tumor necrosis factor α-induced protein 3 mRNA in peripheral blood mononuclear cells negatively correlates with disease severity in psoriasis vulgaris. *Clin. Vaccine Immunol.* **19**, 1938–1942 (2012).
42. Kelly, C. *et al.* Expression of the inflammatory regulator A20 correlates with lung function in patients with cystic fibrosis. *J. Cyst. Fibros.* **12**, 411–415 (2013).
43. Kaiser, W.J. *et al.* RIPK3 mediates the embryonic lethality of caspase-8-deficient mice. *Nature* **471**, 368–372 (2011).
44. Oberst, A. *et al.* Catalytic activity of the caspase-8-FLIP$_L$ complex inhibits RIPK3-dependent necrosis. *Nature* **471**, 363–367 (2011).
45. Zhang, H. *et al.* Functional complementation between FADD and RIPK1 in embryos and lymphocytes. *Nature* **471**, 373–376 (2011).
46. O'Donnell, M.A. *et al.* Caspase 8 inhibits programmed necrosis by processing CYLD. *Nat. Cell Biol.* **13**, 1437–1442 (2011).
47. Moquin, D.M. *et al.* CYLD deubiquitinates RIP1 in the TNFα-induced necrosome to facilitate kinase activation and programmed necrosis. *PLoS ONE* **8**, e76841 (2013).
48. Bertrand, M.J. *et al.* Cellular inhibitors of apoptosis cIAP1 and cIAP2 are required for innate immunity signaling by the pattern recognition receptors NOD1 and NOD2. *Immunity* **30**, 789–801 (2009).
49. Bertrand, M.J. *et al.* cIAP1 and cIAP2 facilitate cancer cell survival by functioning as E3 ligases that promote RIPK1 ubiquitination. *Mol. Cell* **30**, 689–700 (2008).
50. McComb, S. *et al.* cIAP1 and cIAP2 limit macrophage necroptosis by inhibiting Rip1 and Rip3 activation. *Cell Death Differ.* **19**, 1791–1801 (2012).
51. Sun, L. *et al.* Mixed lineage kinase domain-like protein mediates necrosis signaling downstream of RIPK3 kinase. *Cell* **148**, 213–227 (2012).
52. Xie, T. *et al.* Structural insights into RIPK3-mediated necroptotic signaling. *Cell Rep.* **5**, 70–78 (2013).

## ONLINE METHODS

**Mice and *in vivo* experiments.** The generation of mice bearing an *A20*$^{fl}$ allele (*A20*$^{fl}$ mice) has been described[9,13]. Mice lacking *A20* exon 2 specifically in T cells were generated by breeding of *A20*$^{fl}$ mice with transgenic CD4-Cre mice. Mice bearing gene-targeted point mutations in the gene encoding A20 (*A20*$^{OTU}$ mice and *A20*$^{ZF4}$ mice) have been described[19]. *Ripk3*$^{-/-}$ mice were provided by X. Wang. *A20*$^{-/-}$ mice were generated by breeding of *A20*$^{fl}$ mice with B6.EIIA-Cre mice, and subsequent breeding of the progeny to C57BL/6J mice and selection for mice bearing the predicted deletion of *A20* exon 2 but not the EIIA-Cre transgene. *Rag1*$^{-/-}$ mice were from Jackson Labs. All mice were generated and maintained on a C57BL/6 inbred background, and all mouse experiments were performed according to institutional guidelines of the University of California, San Francisco (UCSF).

For antigen-specific T cell responses, naive OT-II CD4$^{+}$ T cells were purified from congenically marked mice by flow cytometry, mixed 1:1, labeled with CFSE (carboxyfluorescein diacetate succinimidyl ester) and adoptively transferred into C57BL/6J mice. Mice were immunized with OVA peptide (amino acids 323–339 (ISQAVHAAHAEINEAGR); 200 mg) and LPS (20 μg) 24 h after cell transfer and were analyzed at various time points. For EAE experiments, mice were immunized with MOG peptide (amino acids 35–55 (MEVGWYRSPFSRVVHLYRNGK); 50 μg) in complete Freund's adjuvant with pertussis toxin (200 ng). Clinical symptoms and histological analyses were performed as described[53].

***In vitro* T cell analysis.** For *in vitro* T cell assays, naive (CD4$^{+}$CD25$^{-}$CD44$^{lo}$CD62L$^{hi}$) T cells were purified by bead enrichment and/or sorted by flow cytometry from spleens and lymph nodes from the appropriate strain(s) of mice before stimulation with plate-bound anti-CD3 (2.5 μg/ml; 145-2C11; UCSF Monoclonal Antibody Core) and anti-CD28 (2 μg/ml; PV-1; UCSF Monoclonal Antibody Core). In addition, mouse IL-12 (20 ng/ml; Peprotech) and anti-IL-4 (10 μg/ml; 11B11; Tonbo) were used for $T_H1$ polarization, while human TGF-β (5 ng/ml; Peprotech), mouse IL-6 (20 ng/ml; Peprotech), anti-IL-4 (10 μg/ml; 11B11; Tonbo) and anti-IFNγ (10 μg/ml; XMG1.2; UCSF Hybridoma Core) were used for $T_H17$ polarization. In selected experiments, T cells were labeled with 3 mM CFSE (Invitrogen). The siRNA-mediated decrease in RIPK3 in Jurkat I9.2 cells (American Type Culture Collectino) was achieved with one pulse of 2200 V and 20 ms, with the Neon Transfection System, according to manufacturer's instructions (Invitrogen).

**Flow cytometry.** The following antibodies were used for flow cytometry (all from BD Bioscience): phycoerythrin-indotricarbocyanine—or allophycocyanin-conjugated anti-CD4 (RM4-5), phycoerythrin-indotricarbocyanine— or allophycocyanin-conjugated anti-CD8 (53-6.7), phycoerythrin-indotricarbocyanine—conjugated anti-CD11b (M1-70), allophycocyanin-conjugated anti-Gr-1 (RB6-8C5), allophycocyanin- or fluorescein isothiocyanate–conjugated anti-CD45.1 (A20), allophycocyanin- or fluorescein isothiocyanate–conjugated anti-CD45.2 (104), fluorescein isothiocyanate–conjugated anti-CD44 (IM-7), phycoerythrin- or allophycocyanin-conjugated anti-CD62L (MEL-14) and fluorescein isothiocyanate–conjugated anti-TCRβ (H57-597). Live cells were quantitated by flow cytometry of cells negative for DAPI (4,6-diamidino-2-phenylindole). For analysis of intracellular cytokine expression, cells were incubated with phorbol 12-myristate 13-acetate (50 ng/ml; Sigma-Aldrich), ionomycin (250 ng/ml; Sigma-Aldrich) and GolgiPlug (1 μl/ml; BD Bioscience) for 4 h before collection. Cells were stained with e450-conjgated anti-CD4 (RM4-5; Tonbo), phycoerythrin-conjugated anti-IFN-γ (XMG1.2; BD Bioscience), Alexa Fluor 647–conjugated anti-IL-17A (TC11-18H10; BD Bioscience), a Live/Dead cell stain kit (Invitrogen) and a Cytofix/Cytoperm kit (BD Bioscience).

**Signaling assays.** Stimulated T cells were incubated in lysis buffer (10 mM Tris HCl, pH 7.4, 150 mM NaCl, 10% glycerol, 1.0% NP-40 supplemented with cOmplete EDTA-Free Protease Inhibitor Cocktail (Roche Applied Science), phosphatase inhibitors (1 mM $Na_3VO_4$, 10 mM NaF and 20 mM β-glycerol phosphate) and 10 mM N-ethylmaleimide). For analysis of signaling complexes, cell lysates were pre-cleared with protein G beads before immunoprecipitation with anti-RIPK1 (D94C12 ; Cell Signaling Technology). Antibodies and reagents used for immunoprecipitation and immunoblotting studies included the following: anti-RIPK1 (38/RIP), anti-Bim (559685) and anti-Bcl-x (610212) (all from BD Bioscience); anti-Bcl-2 (50E3; Cell Signaling Technology); anti-actin (JLA20; EMD Millipore); anti-RIPK3 (2283; ProSci); anti-Bax (B-9; Santa Cruz Biotechnology); anti-RIPK1 (D94C12) and anti-A20 (D13H3) (both from Cell Signaling Technology); and Q-VD and Z-VAD (Enzo Life Science).

Studies of signaling in MEFs were performed as described[19]. RIPK1 was immunoprecipitated with anti-RIPK1 (D94C12; Cell Signaling) and Dynabeads M270 Epoxy (Invitrogen). Proteins containing K63-linked ubiquitin chains were immunoprecipitated with antibody to K63-linked ubiquitin (Apu3; EMD Millipore) and Dynabead Protein A (Invitrogen). RIPK3 mutants were generated by the introduction of mutant RIPK3–encoding cDNA into green fluorescent protein (GFP)-expressing lentiviral constructs, followed by infection of *A20*$^{-/-}$*Ripk3*$^{-/-}$ MEFs with these viruses. Productively infected cells (GFP$^{+}$) cells) were sorted by flow cytometry to obtain pure populations of transduced RIPK3-expressing cells before analysis in necroptosis assays. The survival of MEFs was quantified with the CellTiter-Glo Luminescent Cell Viability Assay according to the manufacturer's instructions (Promega).

**Mass spectrometry.** Pellets of stimulated cells were solubilized in urea, ammonium bicarbonate and 10 mM TCEP (tris(2-carboxyethyl)phosphine), were alkylated with iodoacetic acid and were digested overnight with trypsin modified by TPCK (L-1-tosylamide-2-phenylethyl chloromethyl ketone). Trypsin-treated peptides underwent enrichment for ubiquitinated peptides with a PTMScan Ubiquitin Remnant Motif kit according to the manufacturer's protocol (5562; Cell Signaling Technology). Affinity-purified ubiquitinated peptides were separated by nano-flow liquid chromatography in a 75-μm × 150-mm reverse-phase 1.7-μm BEH 130 C18 column (Waters); the eluate was coupled to an ion trap–Orbitrap mass spectrometer (LTQ Orbitrap Velos; Thermo Scientific); and data were searched against the murine subset of the UniProtKB database with in-house ProteinProspector tools (version 5.8.0). For quantitative (stable isotope labeling) mass spectrometry experiments, *A20*$^{KO2/KO2}$ and *A20*$^{+/+}$ MEFs were passaged in the presence of dialyzed serum supplemented with amino acids labeled with a heavy isotope (*A20*$^{+/+}$) or a light isotope (*A20*$^{KO2/KO2}$) for 2 weeks before stimulation. Lysates from *A20*$^{+/+}$ and *A20*$^{KO2/KO2}$ cells were mixed, treated with trypsin and immunoprecipitated with antibody to di-glycine remnants ('UbiScan') before mass spectrometry analysis[35].

53. Molnarfi, N. *et al.* MHC class II-dependent B cell APC function is required for induction of CNS autoimmunity independent of myelin-specific antibodies. *J. Exp. Med.* **210**, 2921–2937 (2013).





doi:10.1038/ni.3172

# Erratum: The ubiquitin-modifying enzyme A20 restricts ubiquitination of the kinase RIPK3 and protects cells from necroptosis

**Michio Onizawa, Shigeru Oshima, Ulf Schulze-Topphoff, Juan A Oses-Prieto, Timothy Lu, Rita Tavares, Thomas Prodhomme, Bao Duong, Michael I Whang, Rommel Advincula, Alex Agelidis, Julio Barrera, Hao Wu, Alma Burlingame, Barbara A Malynn, Scott S Zamvil & Averil Ma**
***Nat. Immunol.* 16, 618–627 (2015); published online 4 May 2015; corrected after print 21 May 2015**

In the version of this article initially published, the filled circles in Figure 3b were incorrectly labeled '*A20*$^{+/fl}$CD4-Cre'. The correct label is '*A20*$^{fl/fl}$CD4-Cre'. The error has been corrected in the HTML and PDF versions of the article.